




## Open Archive Toulouse Archive Ouverte (OATAO)

OATAO is an open access repository that collects the work of Toulouse researchers and makes it freely available over the web where possible

This is an author's version published in: <http://oatao.univ-toulouse.fr/24654>

**Official URL:** <https://doi.org/10.1016/j.apsusc.2019.01.115>

**To cite this version:**

Parellada-Monreal, Laura and Castro-Hurtado, Irène and Martínez-Calderón, Miguel and Presmanes, Lionel  and Mandayo, Gemma García *Laser-induced periodic surface structures on ZnO thin film for high response NO<sub>2</sub> detection.* (2019) Applied Surface Science, 476. 569-575. ISSN 0169-4332

Any correspondence concerning this service should be sent to the repository administrator: [tech-oatao@listes-diff.inp-toulouse.fr](mailto:tech-oatao@listes-diff.inp-toulouse.fr)

# Laser-induced periodic surface structures on ZnO thin film for high response NO<sub>2</sub> detection

L. Parellada-Monreal<sup>a,b</sup>, I. Castro-Hurtado<sup>a,b</sup>, M. Martínez-Calderón<sup>a,b</sup>, L. Presmanes<sup>c</sup>, G.G. Mandayo<sup>a,b,\*</sup>

<sup>a</sup> Ceit, Manuel Lardizábal 15, 20018 Donostia/San Sebastián, Spain

<sup>b</sup> Universidad de Navarra, Tecnun, Manuel Lardizábal 13, 20018 Donostia/San Sebastián, Spain

<sup>c</sup> CIRMAT, Université de Toulouse, CNRS, INPT, UPS, Toulouse Cedex 9, France

## ARTICLE INFO

### Keywords:

ZnO  
Femtosecond laser  
LIPSS  
Raman  
Gas sensor  
NO<sub>2</sub>

## ABSTRACT

Femtosecond laser-induced periodic structures (LIPSS) have been processed on ZnO thin film gas sensor devices for nitrogen dioxide (NO<sub>2</sub>) detection. From the morphology point of view, the nanostructures have been identified as high spatial frequency LIPSS (HSFL) with an average period of 145 nm. Through Raman analysis, a decrease of the typical wurtzite ZnO structure is shown, with a possible increase of defects such as Zn interstitials. The response under NO<sub>2</sub> is enhanced if compared with the only-annealed ZnO thin film for concentrations as low as 1 ppm, reaching 1 ppb of detection limit (LOD) for the sensors with LIPSS. The Zn interstitials defects could be the source of the adsorbed NO<sub>2</sub> species increasing the sensitivity. Reproducible results have been measured during 11 weeks in a row.

## 1. Introduction

Nanostructured materials present special characteristics due to their small dimensions and morphologies, usually causing exceptional structural [1] and electrical [2] properties. Among others, these qualities are useful for applications such as drug delivery [3], energy conversion [4] or chemical sensors [5]. Specifically on the sensing field, nanostructured materials have been widely investigated since the phenomena involved are based on surface reactions [6,7].

In the case of ZnO, shapes like nanoneedles, nanorods or hierarchical structures have shown great responses to oxidizing gases, specially to NO<sub>2</sub> [8–10]. In this work, femtosecond laser induced periodic structures (LIPSS) have been chosen to modify the sputtered ZnO surface for chemical sensor applications purposes.

LIPSS based nanopatterns consist of a surface relief made of (quasi) periodic lines, which exhibit a clear correlation to the wavelength and polarization of the radiation [11]. Therefore, these structures are generated when linearly polarized radiation interacts with a solid. Recently, femtosecond LIPSS has proven its potential in patterning metallic materials [12], dielectrics [13], polymers [14] and thin films [15].

Compared to traditional laser ablation techniques, femtosecond laser nano machining delivers extreme peak irradiance with minimal

thermal effects, offering the possibility of surface processing in open air atmosphere avoiding expensive vacuum technologies, while being free of chemicals and relatively fast. One of the most attractive properties of LIPSS based patterning is that is highly controllable, since it mainly depends on the material in use, the laser wavelength,  $\lambda$ , the number of applied pulses per spot,  $N$ , the angle of incidence,  $\theta$ , and the polarization state of the laser electric field [16,17].

In terms of nano structure periodicity,  $\Lambda$ , LIPSS are divided into two main groups: the ones with  $\Lambda$  close to the irradiation wavelength are called low spatial frequency LIPSS (LSFL), while structures with periods significantly smaller than  $\lambda$  are referred to as high spatial frequency LIPSS (HSFL) [11,18].

The existence of HSFL allows for the generation of much smaller periods than LSFL, down to  $\sim \lambda/4 - \lambda/8$ , and although their origin is not fully understood and controversially debated in the literature [19,20], these structures have been obtained in a wide number of materials by carefully tuning the laser processing parameters. HSFL are formed at fluences very close to the damage threshold of the irradiated material and are oriented either parallel or perpendicular to the laser beam polarization, depending on the material [11].

As far as we are concerned, LIPSS have not been used as a crystallographic and morphology modification for a possible enhancement of the gas sensing response. Due to the changes on the surface structure,

\* Corresponding author at: Ceit, Manuel Lardizábal 15, 20018 Donostia/San Sebastián, Spain.

E-mail address: [gmandayo@ceit.es](mailto:gmandayo@ceit.es) (G.G. Mandayo).

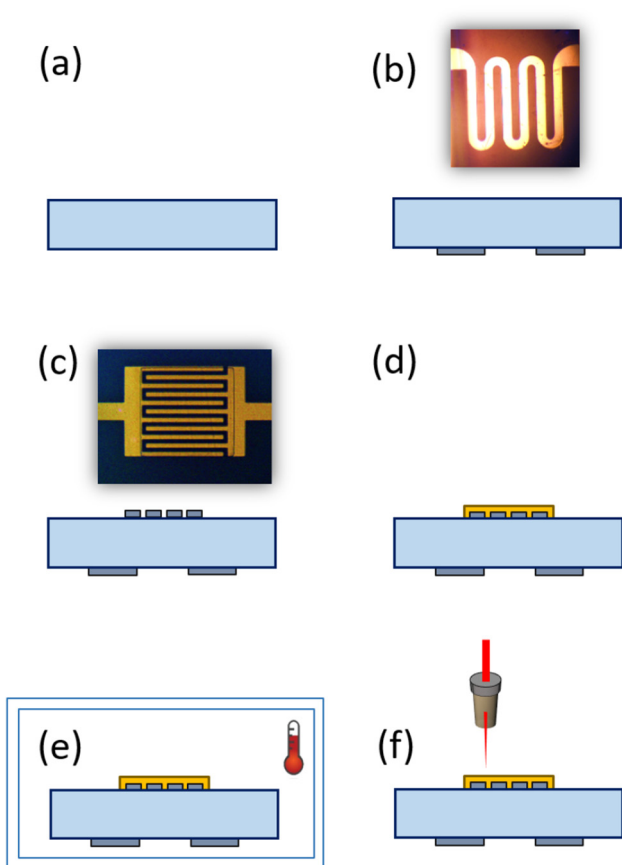


**Fig. 1.** Sensor fabrication steps: (a) alumina substrate, (b) Pt heater deposited on the back side of the alumina substrate, (c) Pt IDT electrodes deposited on top of the alumina substrate, (d) ZnO thin film layer deposited on top of the electrodes, (e) thermal treatment at 800 °C and (f) femtosecond laser processing.

defects could be generated at the surface of the semiconductor and consequently a higher response could be expected for specific gases. Besides, the generation of LIPSS with a femtosecond laser presents an important advantage for gas sensing applications since the nanostructures can be patterned directly on the sensing device (in situ),

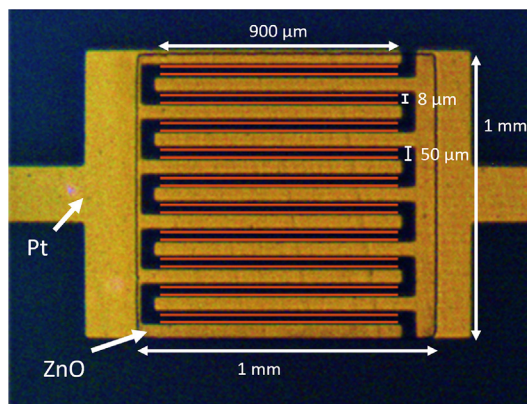


**Fig. 3.** Optical image of the IDT Pt electrodes with the ZnO thin film on top. The dimensions of the LIPSS lines are not to scale with the rest of the image.

without the need to transfer them, as it is the case of most of bottom up techniques (ex situ) such as electrospinning [21] or hydrothermal [22] methods. On the other hand, this laser technique is able to nanostructure large surface areas [17], what is an important issue for its application in industrial processes.

In particular, in this work, sputtered ZnO thin films, a semiconductor that is well known as a sensitive layer for chemoresistive gas sensors, have been processed with a femtosecond laser in order to generate LIPSS on its surface. The device has been tested under different atmospheres and specially under NO<sub>2</sub>, to study the nanostructures effect compared to only annealed thin films.

## 2. Experimental

### 2.1. Sensor fabrication

The fabrication steps of the ZnO sensing device are summarized in Fig. 1. The sensor is based on a 1 × 2 cm<sup>2</sup> polished alumina substrate, where a Pt heater was fabricated at the back side by photolithography followed by DC sputtering in an Edwards ESM 100 system (Fig. 1(b)). The lift off process was carried out with acetone. The same fabrication steps were used to fabricate Pt interdigitated (IDT) electrodes with 50 μm of separation and width on the top surface of the alumina

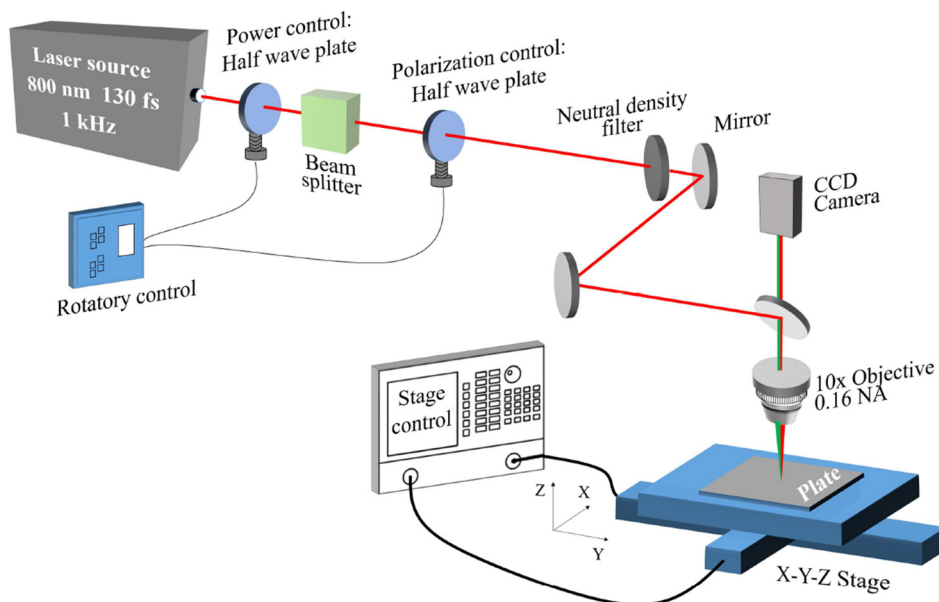


**Fig. 2.** Schematic layout of the femtosecond laser machining setup for processing ZnO thin film at 800 nm.

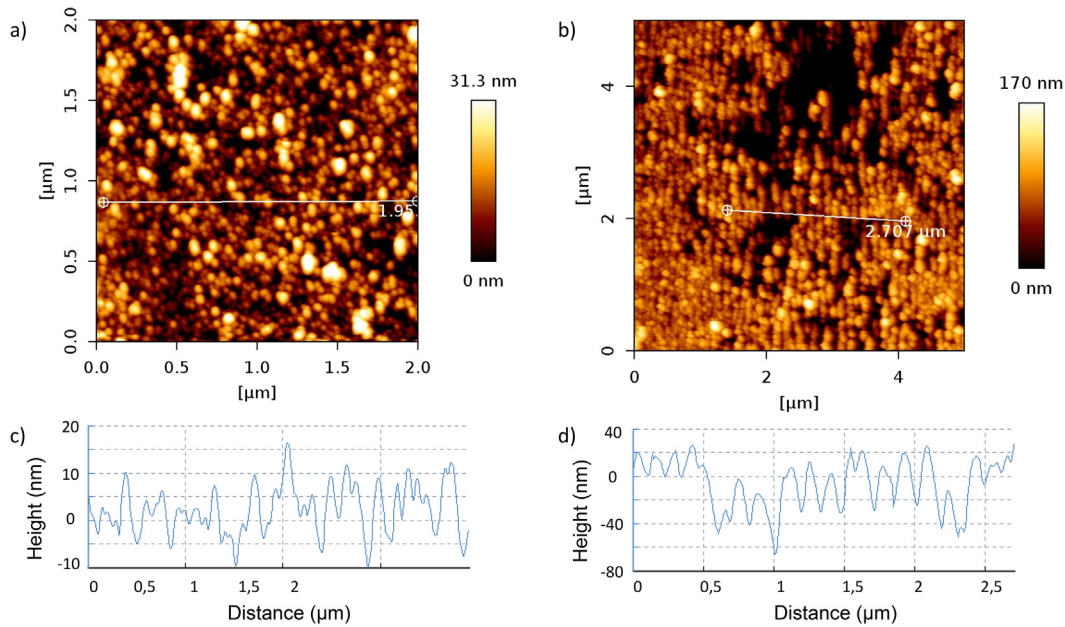


Fig. 4. (a)  $2 \mu\text{m}^2$  AFM tapping mode images of ZnO TT800C on alumina, (b)  $5 \mu\text{m}^2$  AFM tapping mode images of ZnO TT800C + LIPSS on alumina, (c) section profile of the ZnO TT800C grains and (d) section profile of the LIPSS.

(Fig. 1(c)). In order to improve the adhesion of the metal to the substrate, a 25 nm thick Cr layer was deposited for the subsequent 200 nm thick Pt sputtering, both in the heater and in the IDT electrodes.  $1 \text{ mm}^2$  of ZnO sensing layer was deposited on top of the Pt IDT electrodes by photolithography followed by RF sputtering in an Argon atmosphere (ZnO target 99.999% purity) under  $5 \cdot 10^{-3}$  mbar of gas pressure in a Pfeiffer Iontech system. The ZnO sputtering time was 1 h, the deposition temperature was between  $21^\circ\text{C}$  and  $23^\circ\text{C}$  and as for the Pt, acetone was used for the lift off process (Fig. 1(d)). Afterwards, as shown in (Fig. 1(e)), the sensor device was thermally stabilized in a quartz oven at  $800^\circ\text{C}$  during 4 h in synthetic air (this process will be named TT800C). Finally, the femtosecond laser processing for the LIPSS generation was performed (Fig. 1(f)).

The laser system used to generate the LIPSS on the ZnO surface was a Ti:Sapphire mode locked oscillator with a regenerative amplifier able to generate 130 fs pulses at a central wavelength of 800 nm with a 1 kHz repetition rate. The specific set up is shown in Fig. 2. The laser spot was focused on the ZnO samples utilizing a broadband  $10\times$  microscope objective with a numerical aperture (NA) of 0.16. Then, the spot size on the samples was measured using a  $50\times$  microscope objective and a Coherent LaserCam HR UV, yielding approximately a focused spot diameter ( $\omega_0$ ) of  $6 \mu\text{m}$  at 800 nm. Also, in the experiments of this work, the focusing point was displaced certain distances yielding to different values of the spot diameter ( $\omega_z$ ) and consequently machined line width [23].

In order to obtain the optimum laser parameters for LIPSS fabrication, different values of laser scanning velocity, pulse energy and spot diameter were tested. The scanning velocity tested were  $5 \mu\text{m/s}$ ,  $10 \mu\text{m/s}$ ,  $20 \mu\text{m/s}$  and  $50 \mu\text{m/s}$ , the pulse energies tested were  $0.1 \mu\text{J}$ ,  $0.5 \mu\text{J}$  and  $1 \mu\text{J}$  and the spot diameters were varied from  $6 \mu\text{m}$  up to  $40 \mu\text{m}$  by displacing the focusing point. These parameter combinations lead to the fabrication of LIPSS with different morphologies that were characterized via FEG SEM. Among all of them, using a pulse energy of  $0.5 \mu\text{J}$ , scanning speed of  $10 \mu\text{m/s}$  and the laser beam focused to a  $\omega_0$  of  $7 \mu\text{m}$  approximately, allowed us to fabricate the LIPSS nanopatterns with higher homogeneity and definition.

On the ZnO surface, two consecutive lines of LIPSS  $900 \mu\text{m}$  long and separated  $8 \mu\text{m}$  were written between each IDT electrode as indicated in red in Fig. 3. The femtosecond laser processed only regions of ZnO thin film deposited directly over the alumina substrate and not over the Pt

IDT in order to avoid alteration of the Pt/ZnO interface.

## 2.2. Film characterization

The ZnO thin film thickness, measured with a KLA Tencor profilometer, was around 180 nm.

To study the surface topography a JPK Nanowizard 3 Atomic Force Microscope (AFM) was used. Tapping Mode images were obtained using silicon Tap300 G cantilevers with a resonance frequency around 300 kHz and a tip with a radius  $<10 \text{ nm}$ .

A Scanning Electron Microscope (SEM) Quanta 3D Field Emission Gun (FEG) system supplied by FEI Company was used to study the LIPSS morphology surface and in depth. The LIPSS periods were analyzed using the two dimensional Fast Fourier Transforms (2D FFT) of the FEG SEM surface images.

Raman spectra were collected under ambient conditions using Horiba Jobin Yvon LabRAM HR 800 spectrometer equipped with a fiber coupled 532 nm laser. Spectra acquisition was carried out for 300 s using a  $\times 100$  objective lens and 1800 gr/mm grating. During the measurement, the resulting laser power at the surface of the sample was adjusted to 4 mW.

## 2.3. Electrical characterization

The electrical response characterization of the sensors under different gases was carried out inside a sealed stainless steel chamber. The  $\text{NO}_2$ , carbon monoxide (CO), benzene ( $\text{C}_6\text{H}_6$ ), vinyl chloride ( $\text{C}_2\text{H}_3\text{Cl}$ ) and chlorine ( $\text{Cl}_2$ ) gases were taken from certified bottles mixed with synthetic air (Air Liquide) in concentrations of 50, 100, 20, 10 and 15 ppm, respectively. In all the experiments a total flux of 400 sccm was used. The gas mixture in the chamber was obtained by a system consisting of a PC controlled mass flow controllers (MFCs) Bronkhorst Hi Tech. A DDE (Dynamic Data Exchange) communication is established between the computer and the MFCs by Labview<sup>®</sup>.

The power consumption of the Pt heating element has been doubly calibrated with a thermographic camera and a Pt100 resistor, so the heater is power controlled by a voltage source. The conductance variation of the sensing element was measured with a Keithley 2000 Multimeter, controlled by Labview<sup>®</sup> via GPIB.

The response of the sensors ( $\text{SR}_x$ , where x is the name of the gas)

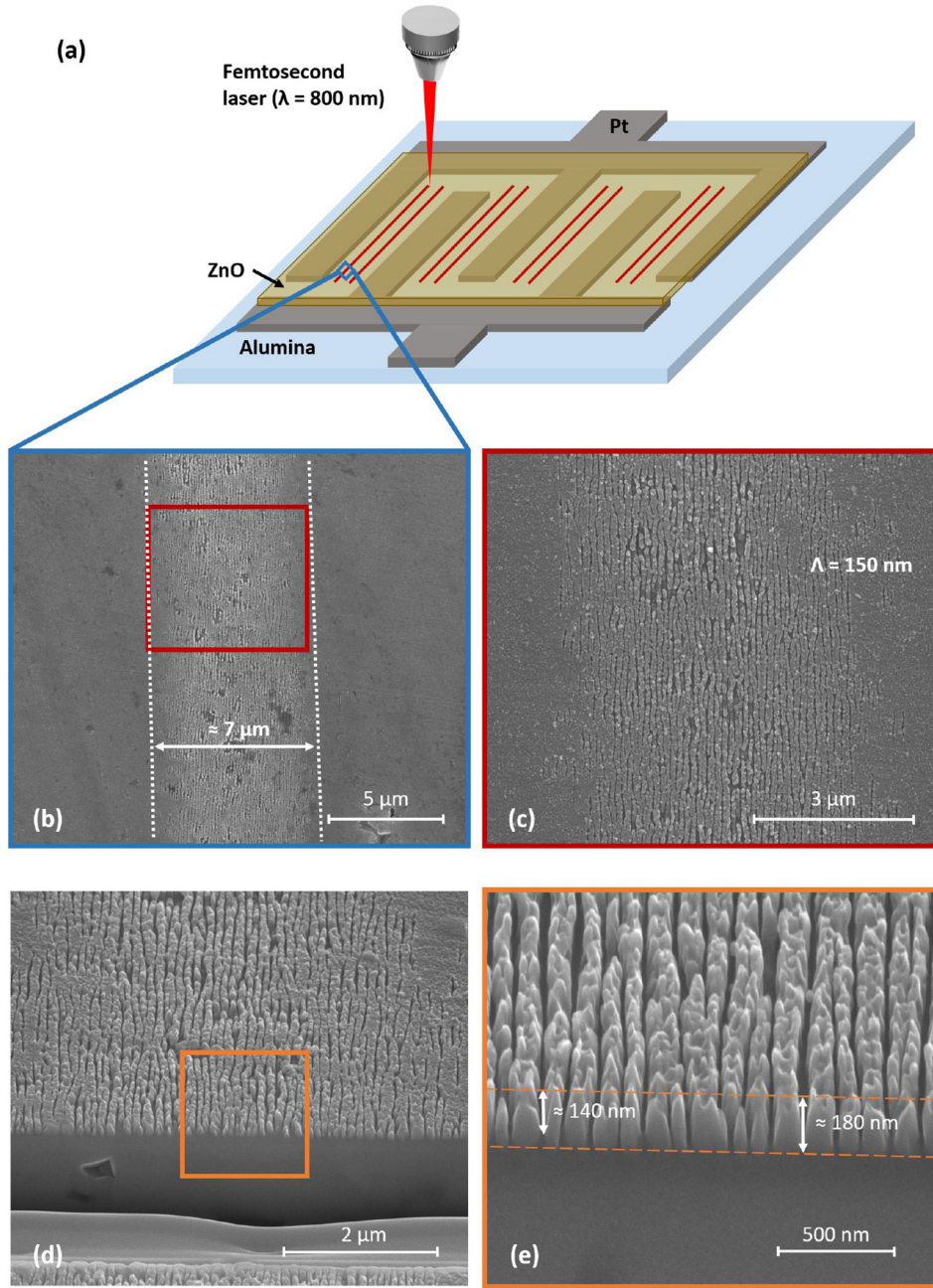


**Fig. 5.** (a) Schematic draw of the Pt IDT electrodes with the ZnO thin film on top. The red lines represent the LIPSS structures. (b) SEM image of one LIPSS line, (c) zoomed image of (b), (d) SEM image of a cross-section of the ZnO LIPSS processed by femtosecond laser and (e) zoomed image of (d).

was calculated using the following definitions:

$$SR_x = G_{air}/G_{gas} \quad (1)$$

$$SR_x = G_{gas}/G_{air} \quad (2)$$

for oxidizing and reducing agents respectively, where  $G_{air}$  is the conductivity of the sensor in air, and  $G_{gas}$  represents the sensor conductivity after 30 min of gas exposure. The conductivity is defined as the inverse of the resistance.

### 3. Results and discussion

#### 3.1. LIPSS nanostructuring characterization

From AFM and SEM images, a periodic structure can be observed in Figs. 4(b) and 5. The average period of the nanostructures extracted

from the 2D FFT is 145 nm and the average width of the processed lines is around 7  $\mu\text{m}$  (Fig. 5). From the profiles of some AFM images (Fig. 4(d)) a LIPSS depth around 100 nm is observed, while the average depth in the SEM cross section of the LIPSS is 140 nm. This mismatching between both measurements could be due to the fact that the tip of the cantilever has a radius of curvature ( $r < 10$  nm) and pyramidal shape, being unable to reach the bottom of the ZnO surface, implying an underestimation of the LIPSS height.

Taking into account the length and the approximate width of the lines generated with LIPSS, a 12.5% of the total ZnO thin film surface was processed.

The granular morphology and the size of the grains are preserved under the LIPSS as can be appreciated in Fig. 4(a) and (b) (it is worth to notice that the AFM scanned areas have different size in each image). The average grain size is about 42 nm of diameter.

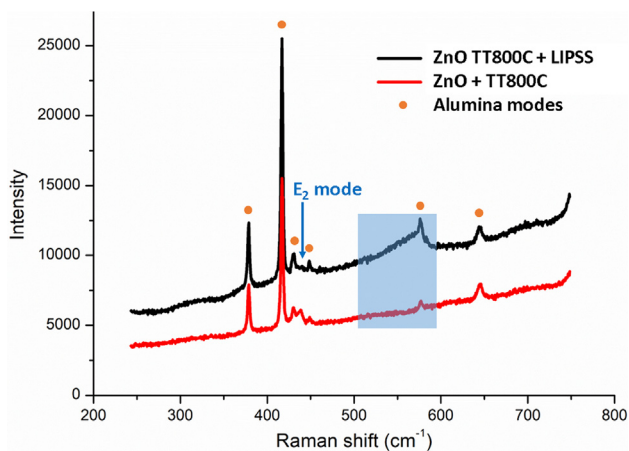


**Fig. 6.** Raman spectra of ZnO thin film annealed at 800 °C compared with ZnO thin film annealed at the same temperature with LIPSS.

**Table 1**

Ratios between the NO<sub>2</sub> response and the rest of the gases.

	$\frac{SR_{NO_2}}{SR_{NO_2}}$	$\frac{SR_{NO_2}}{SR_{CO}}$	$\frac{SR_{NO_2}}{SR_{C_6H_6}}$	$\frac{SR_{NO_2}}{SR_{C_2H_3Cl}}$	$\frac{SR_{NO_2}}{SR_{Cl_2}}$
TT800C + LIPSS	1	2.52	2.47	2.47	2.45
TT800C	1	1.70	1.57	1.62	1.64

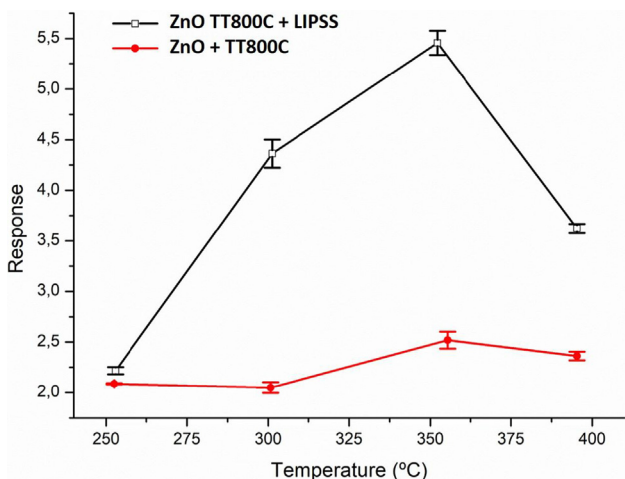


**Fig. 7.** Response ( $SR_{NO_2}$ ) of the ZnO sensors with LIPSS and without as a function of temperature for 2 ppm of NO<sub>2</sub>.

In the specific case of ZnO nanostructuring via LIPSS, the existence of HSFL and LSFL has been thoroughly analyzed by Pin Feng et al. [24]. In this work, the generation of HSFL with a periodicity of approximately 145 nm has been shown. This result is in agreement also with the observations of X. D. Guo et al. [25,26] and M. Zamfirescu [27]. Regarding the established classification of HSFL in the work of J. Bonse [11], we suggest that the fabricated structures consist in type HSFL 1 which are mainly observed in dielectrics and semiconductors with a period smaller than half of the incident laser wavelength and a depth of a few tens of nanometers.

Raman measurements were performed in order to investigate the crystallographic modifications between only annealed ZnO thin film and ZnO with LIPSS. As shown in Fig. 6, the Raman peaks that are common in both samples (378, 416, 430, 445, 576 and 645 cm<sup>-1</sup>) are identified with the alumina substrate [28]. From the ZnO, it can be observed that the peak around 436 cm<sup>-1</sup> vanishes for the ZnO with LIPSS. This peak is identified with the optical phonon E<sub>2</sub> mode and

attributed to the wurtzite crystal structure of ZnO [29], indicating that on the LIPSS the wurtzite structure quality diminishes. This effect also matches with the results shown by the team of X. D. Guo [25], where ZnO nanostructures have been processed with a similar setup.

The sharp peak present in both samples at 576 cm<sup>-1</sup> is related to a Raman mode of the alumina substrate, as mentioned before. However, there exists another very broad peak on the ZnO with LIPSS, between 518 cm<sup>-1</sup> and 594 cm<sup>-1</sup>, approximately (highlighted in blue square in Fig. 6). A similar wide peak is shown in the Raman spectra of the LIPSS nanostructures generated by X. D. Guo with a maximum around 570 cm<sup>-1</sup> and they attribute it to ZnO A1(LO) phonon mode, related to the defects of the nanostructures due to the laser irradiation. Nevertheless, in the work done by G. J. Exarhos [29] on ZnO films is proposed that a peak around 579 cm<sup>-1</sup>, identified with the E1(LO) mode, could be related to defect electronic states within the bandgap due to an excess of Zn content in the film. In the work of K. Saw [30], where characterization of ZnO thin films is carried out, the same peak appears wider (from 530 cm<sup>-1</sup> to 620 cm<sup>-1</sup>) and is also identified with the same kind of defects and contrasted with X ray Photoelectron Spectroscopy (XPS) analysis. Besides, in the characterization of ZnO multi layer nanosheets [31] a peak at 560 cm<sup>-1</sup> is related to Zn existence due to incomplete oxidation. Therefore, it can be concluded that the wide peak that appears on the Raman spectra of the LIPSS nanostructures is related with defects, possibly due to Zn interstitials.

### 3.2. Gas sensing results

The detection principle of chemical gas sensors is based on the rise or decrease of the sensing material conductivity when it is exposed to reducing or oxidizing atmospheres. The sensing material needs to be heated up to temperatures around 200 °C 400 °C, where oxygen in the form of negatively charged species adsorbs on the surface of the semiconductor.

To demonstrate the sensing properties of the LIPSS generated on the ZnO thin film, sensor devices with and without LIPSS were measured at a typical detection temperature (325 °C) under 5 ppm of NO<sub>2</sub>, 50 ppm of CO, 5 ppm of C<sub>6</sub>H<sub>6</sub>, 10 ppm of C<sub>2</sub>H<sub>3</sub>Cl and 1 ppm Cl<sub>2</sub> mixed with air. Preliminary results showed that the only oxidizing gas tested, NO<sub>2</sub>, presents the highest response for both type of sensors. In Table 1 the different  $\frac{SR_{NO_2}}{SR_x}$  ratios have been calculated, showing a very good selectivity to NO<sub>2</sub>, specially for TT800C + LIPSS, regarding the other reducing agents.

Therefore, a deep study has been carried out with the NO<sub>2</sub> gas. In Fig. 7, the response of both type of sensors at different temperatures are shown for 2 ppm of NO<sub>2</sub>. As can be appreciated, the sensors with LIPSS present responses much higher than non processed ZnO thin film, although the error bars are slightly bigger for all the temperatures in the case of the sensor processed by the femtosecond laser. All the error bars are calculated using four different measurements. Taking into account the abrupt increase in response around 350 °C, this temperature has been considered as the optimal temperature.

Afterwards, at the optimal temperature, the sensors were exposed to different concentrations in order to study the sensitivity of the devices (Fig. 8). For all tested concentrations (5 ppm, 2 ppm and 1 ppm) of NO<sub>2</sub>, the sensor processed with LIPSS presents a higher response than the ZnO thin film. In addition, repeatability of the response under 2 ppm is tested, showing the same response at nonconsecutive pulses. In Fig. 8(b), a linear sensitivity is shown for both sensors for concentrations between 5 and 1 ppm of NO<sub>2</sub>, so it can be calculated from the slope of the straight line. The sensitivities are 1.7 and 0.8 ppm<sup>-1</sup> for the sensor with LIPSS and without them, respectively. The detection limit (LOD) has been calculated using the following formula:  $LOD = 3\sigma/b$  where  $\sigma$  is the standard deviation of the base line during 5 min and  $b$  is the calculated sensitivity. For the sensor without LIPSS the LOD is already good: 3 ppb, but for the sensor with LIPSS, the theoretical LOD

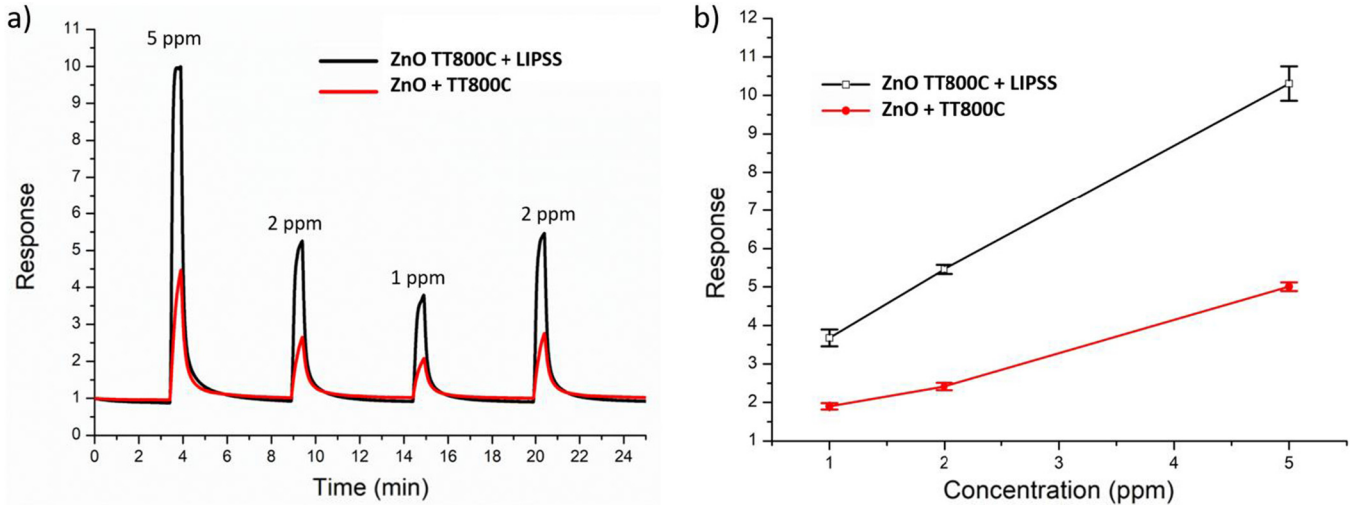


**Fig. 8.** (a) Response ( $SR_{NO_2}$ ) of the ZnO sensors with LIPSS and without at the optimal temperature ( $T_{opt} \approx 350^\circ C$ ) for 5, 2, 1 and 2 ppm of  $NO_2$ . (b) Sensitivity of the two sensors at the optimal temperature.

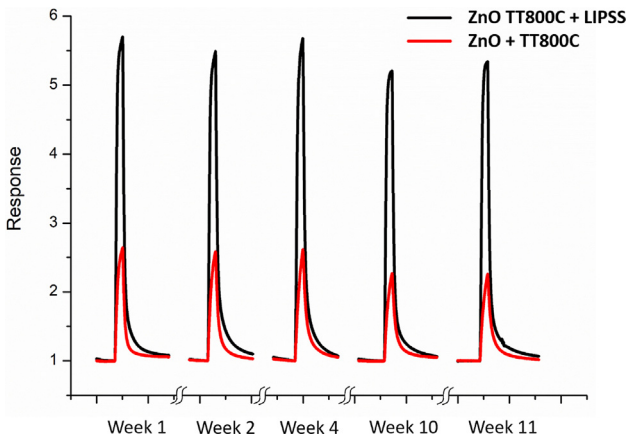


**Fig. 9.** Repeatability of the responses ( $SR_{NO_2}$ ) of both sensors under exposure of 2 ppm of  $NO_2$  measured during several weeks in a row.

downs to 1 ppb, showing up the possibility to use it in hazardous environments.

In order to study the repeatability of the sensors, pulses of 2 ppm of  $NO_2$  during 30 min have been carried out every week, during 4 weeks in a row. After a month and a half with the sensors kept in the chamber open to ambient air and at the optimal temperature, the same experiment was performed and results are shown in Fig. 9. Both kind of sensors present a repeatable behavior over all the tested period, with a repeatability standard deviation ( $S_r$ ) of 0.21 and 0.19 for the sensor with and without LIPSS, respectively. The consequent repeatability values ( $r = 2.3 \times S_r$ ) are 0.48 and 0.44, respectively.

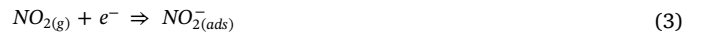
The responses showed for the sensor processed with LIPSS towards low concentrations of  $NO_2$  are similar or higher compared with other published pure ZnO nanostructured sensors such as [32,22,33]. Although in the other works, the optimal temperatures are slightly lower than for the sensor with LIPSS, the fabrication techniques require several steps avoided here by the in situ nanostructuring and selectivity is not shown in any of the investigations. Moreover, repeatability measurements are rarely performed, leading to a lack of information and in this work we successfully demonstrate a good repeatability over more than two months, what is a key requirement for real applications.

During all the gas measurements performed at the optimal temperature, the resistance baseline in the presence of air of the two type of sensors varied in the range of 20 k $\Omega$  80 k $\Omega$  and 3 k $\Omega$  18 k $\Omega$  for the sensor processed with LIPSS and for the sensors only annealed,

respectively.

Many conductometric  $NO_2$  sensor devices have been tested during the last decade, as it can cause severe respiratory diseases for long exposures, but the  $NO_2$  detection mechanism in semiconductors is still under investigation [34].

Most of the proposed mechanisms are based on the importance of the donor concentration defects, since can give electrons to  $NO_2$  molecules, decreasing the carrier density of the semiconductor. Two main possible reactions are involved during the process [35,21]:



where  $NO_2$  in gas form reacts directly with the semiconductor surface, generating adsorbed  $NO_2$  species (3) or NO gas molecules and oxygen species (4). Aside from  $NO_{2(ads)}^-$ , other adsorbed  $NO_2$  species could be generated, as it is explained in [36], always through an electron given from a donor defect to a  $NO_2$  molecule with a simultaneous reoxidation of an oxygen vacancy or Zn interstitial [37]. It is accepted that reaction (3) occurs for temperatures lower than 250  $^\circ C$  and reaction (4) for higher temperatures [35], therefore at the optimal temperature of the sensors presented here, the reaction (4) should take place.

In ZnO nanoparticles, defects detected by photoluminescence (PL) have been identified to contribute to the  $NO_2$  detection mechanism [38]. More specifically, the group of M. Chen highlighted the effect of donor defects as well as surface oxygen species [39,36] through in situ diffuse reflectance infrared fourier transform spectroscopy (DRIFTS) technique. As a result, it is proposed that the increase in response of the ZnO sensor devices with LIPSS nanostructures on it, compared with only annealed ZnO thin film, could be a consequence of the increase of the Zn interstitials defects on the ZnO surface, as Raman measurements suggest. As explained, the sensor processed with LIPSS present always a higher resistance than the only annealed sensor, what bears out the presence of more Zn interstitials. Therefore, as more donor defects, more electrons will be transferred from the crystal to  $NO_2$  molecules, improving the sensitivity.

#### 4. Conclusions

Generating LIPSS with a femtosecond laser on the ZnO surface is an innovative technique able to modify the surface morphology and the defects at the material's surface. This can be used as an advantage to improve the sensitivity of conductometric gas sensing devices.

In this work, ZnO HSFL nanostructures have been processed on

sensor devices and tested under different gas atmospheres. A good selectivity towards NO<sub>2</sub> gas is shown for both type of sensors compared to CO, C<sub>6</sub>H<sub>6</sub>, C<sub>2</sub>H<sub>3</sub>Cl and Cl<sub>2</sub>. With only a 12.5% of the total ZnO area processed with LIPSS, an increase of the sensor response of 50% (for 2 ppm of NO<sub>2</sub> at 350 °C) is found in comparison with the only annealed ZnO thin film sensor. The LOD downs to 1 ppb for the processed sensor, 3 times higher than for the sensor without LIPSS. With a femtosecond laser with a repetition rate of 1 MHz, instead of 1 kHz, an area of 20.000 μm<sup>2</sup> could be processed in 0.28 s instead of 4.76 min, what could be scalable to mass production.

Raman characterization reveals a decrease of the ZnO wurtzite structure for LIPSS, with an increase of surface defects such as Zn interstitials. Donor defects contribute on the NO<sub>2</sub> detection mechanism, releasing electrons to the oxidizing pollutants and consequently increasing the sensitivity. Consequently, Zn interstitials are proposed as the cause of the response enhancement for the tested NO<sub>2</sub> concentrations.

## Acknowledgements

Funding for this work was provided by the Ministry of Economy and Competitiveness (MINECO) through the TEMIN AIR+ (project n°. TEC2016 79898 C6 3 R) and by the Basque Government under the Elkartek program (MICRO4FAB grant n°. KK 2016 00030). All the authors thank the technical and human support provided by Facility of Analysis and Characterization of Solids and Surfaces of SAIUEX UEX for the FIB measurements.

## References

- [1] V. Roy, A. Djurišić, W. Chan, J. Gao, H. Lui, C. Surya, Luminescent and structural properties of ZnO nanorods prepared under different conditions, *Appl. Phys. Lett.* 83 (1) (2003) 141–143.
- [2] E. Comini, V. Guidi, C. Malagù, G. Martinelli, Z. Pan, G. Sberveglieri, Z.L. Wang, Electrical properties of tin dioxide two-dimensional nanostructures, *J. Phys. Chem. B* 108 (6) (2004) 1882–1887.
- [3] M. Goldberg, R. Langer, X. Jia, Nanostructured materials for applications in drug delivery and tissue engineering, *J. Biomater. Sci. Polym. Ed.* 18 (3) (2007) 241–268.
- [4] A.S. Arico, P. Bruce, B. Scrosati, J.-M. Tarascon, W. Van Schalkwijk, Nanostructured materials for advanced energy conversion and storage devices, *Nat. Mater.* 4 (5) (2005) 366.
- [5] X.-J. Huang, Y.-K. Choi, Chemical sensors based on nanostructured materials, *Sens. Actuat. B: Chem.* 122 (2) (2007) 659–671.
- [6] S.R. Morrison, Semiconductor gas sensors, *Sens. Actuat.* 2 (1981) 329–341.
- [7] C. Wang, L. Yin, L. Zhang, D. Xiang, R. Gao, Metal oxide gas sensors: sensitivity and influencing factors, *Sensors* 10 (3) (2010) 2088–2106.
- [8] J. Gonzalez-Chavarri, L. Parellada-Monreal, I. Castro-Hurtado, E. Castaño, G.G. Mandayo, ZnO nanoneedles grown on chip for selective NO<sub>2</sub> detection indoors, *Sens. Actuat. B: Chem.* 255 (2018) 1244–1253.
- [9] M. Jiao, N.V. Chien, N. Van Duy, N.D. Hoa, N. Van Hieu, K. Hjort, H. Nguyen, On-chip hydrothermal growth of ZnO nanorods at low temperature for highly selective NO<sub>2</sub> gas sensor, *Mater. Lett.* 169 (2016) 231–235.
- [10] Y. Navale, S. Navale, N. Ramgir, F. Stadler, S. Gupta, D. Aswal, V. Patil, Zinc oxide hierarchical nanostructures as potential NO<sub>2</sub> sensors, *Sensors Actuat. B: Chem.* 251 (2017) 551–563.
- [11] J. Bonse, S. Höhm, S.V. Kirner, A. Rosenfeld, J. Krüger, Laser-induced periodic surface structures—a scientific evergreen, *IEEE J. Sel. Top. Quantum Electron.* 23 (3) (2017) 109–123.
- [12] M. Martínez-Calderon, M. Manso-Silván, A. Rodríguez, M. Gómez-Aranzadi, J. García-Ruiz, S. Olaizola, R. Martín-Palma, Surface micro- and nano-texturing of stainless steel by femtosecond laser for the control of cell migration, *Sci. Rep.* 6 (2016) 36296.
- [13] E. Granados, M. Martínez-Calderon, M. Gomez, A. Rodriguez, S.M. Olaizola, Photonic structures in diamond based on femtosecond uv laser induced periodic surface structuring (LIPSS), *Opt. Express* 25 (13) (2017) 15330–15335.
- [14] E. Rebolgar, M. Castillejo, T.A. Ezquerro, Laser induced periodic surface structures on polymer films: from fundamentals to applications, *Eur. Polym. J.* 73 (2015) 162–174.
- [15] A. Rodríguez, M.C. Morant-Miñana, A. Dias-Ponte, M. Martínez-Calderón, M. Gómez-Aranzadi, S.M. Olaizola, Femtosecond laser-induced periodic surface nanostructuring of sputtered platinum thin films, *Appl. Surf. Sci.* 351 (2015) 135–139.
- [16] J. Bonse, J. Krüger, S. Höhm, A. Rosenfeld, Femtosecond laser-induced periodic surface structures, *J. Laser Appl.* 24 (4) (2012) 042006.
- [17] I. Gnilytskyi, T.J.-Y. Derrien, Y. Levy, N.M. Bulgakova, T. Mocek, L. Orazi, High-speed manufacturing of highly regular femtosecond laser-induced periodic surface structures: physical origin of regularity, *Sci. Rep.* 7 (1) (2017) 8485.
- [18] F.A. Müller, C. Kunz, S. Gräf, Bio-inspired functional surfaces based on laser-induced periodic surface structures, *Materials* 9 (6) (2016) 476.
- [19] M. Huang, F. Zhao, Y. Cheng, N. Xu, Z. Xu, Mechanisms of ultrafast laser-induced deep-subwavelength gratings on graphite and diamond, *Phys. Rev. B* 79 (12) (2009) 125436.
- [20] A. Borowiec, H. Haugen, Subwavelength ripple formation on the surfaces of compound semiconductors irradiated with femtosecond laser pulses, *Appl. Phys. Lett.* 82 (25) (2003) 4462–4464.
- [21] M. Hjiri, L. El Mir, S.G. Leonardi, N. Donato, G. Neri, Co and NO<sub>2</sub> selective monitoring by ZnO-based sensors, *Nanomaterials* 3 (3) (2013) 357–369.
- [22] M. Procek, A. Stolarczyk, T. Pustelny, Impact of temperature and UV irradiation on dynamics of NO<sub>2</sub> sensors based on ZnO nanostructures, *Nanomaterials* 7 (10) (2017) 312.
- [23] J. Alda, *Laser and Gaussian Beam Propagation and Transformation* vol. 2013, (2003) pp. 999–1013.
- [24] P. Feng, L. Jiang, X. Li, K. Zhang, X. Shi, B. Li, Y. Lu, Femtosecond laser-induced subwavelength ripples formed by asymmetrical grating splitting, *Appl. Surf. Sci.* 372 (2016) 52–56.
- [25] X.D. Guo, R.X. Li, Y. Hang, Z.Z. Xu, B.K. Yu, H.L. Ma, X.W. Sun, Raman spectroscopy and luminescent properties of ZnO nanostructures fabricated by femtosecond laser pulses, *Mater. Lett.* 61 (23–24) (2007) 4583–4586.
- [26] X.D. Guo, R.X. Li, Y. Hang, Z.Z. Xu, B.K. Yu, Y. Dai, B. Lu, X.W. Sun, Coherent linking of periodic nano-ripples on a ZnO crystal surface induced by femtosecond laser pulses, *Appl. Phys. A: Mater. Sci. Process.* 94 (2) (2009) 423–426, <https://doi.org/10.1007/s00339-008-4838-y>.
- [27] M. Zamfirescu, M. Ulmeanu, F. Jipa, O. Cretu, A. Moldovan, G. Epurescu, M. Dinescu, R. Dabu, Femtosecond laser induced periodic surface structures on ZnO thin films, *J. Laser Micro Nanoeng.* 4 (1) (2009) 7–10.
- [28] C. Bundesmann, N. Ashkenov, M. Schubert, D. Spemann, T. Butz, E. Kaidashev, M. Lorenz, M. Grundmann, Raman scattering in ZnO thin films doped with Fe, Sb, Al, Ga, and Li, *Appl. Phys. Lett.* 83 (10) (2003) 1974–1976.
- [29] G.J. Exarhos, S.K. Sharma, Influence of processing variables on the structure and properties of ZnO films, *Thin Solid Films* 270 (1–2) (1995) 27–32.
- [30] K.G. Saw, K. Ibrahim, Y.T. Lim, M.K. Chai, Self-compensation in ZnO thin films: an insight from X-ray photoelectron spectroscopy, Raman spectroscopy and time-of-flight secondary ion mass spectroscopy analyses, *Thin Solid Films* 515 (5) (2007) 2879–2884, <https://doi.org/10.1016/j.tsf.2006.08.047>.
- [31] H. Fan, R. Scholz, F. Kolb, M. Zacharias, U. Gösele, F. Heyroth, C. Eischmidt, T. Hempel, J. Christen, On the growth mechanism and optical properties of ZnO multi-layer nanosheets, *Appl. Phys. A* 79 (8) (2004) 1895–1900.
- [32] X. Wang, F. Sun, Y. Duan, Z. Yin, W. Luo, Y. Huang, J. Chen, Highly sensitive, temperature-dependent gas sensor based on hierarchical ZnO nanorod arrays, *J. Mater. Chem. C* 3 (43) (2015) 11397–11405.
- [33] V.L. Patil, S.A. Vanalakar, P.S. Patil, J.H. Kim, Fabrication of nanostructured ZnO thin films based NO<sub>2</sub> gas sensor via SILAR technique, *Sens. Actuat. B: Chem.* 239 (2017) 1185–1193.
- [34] A. Tamvakos, K. Korir, D. Tamvakos, D. Calestani, G. Cicero, D. Pullini, NO<sub>2</sub> gas sensing mechanism of ZnO thin-film transducers: physical experiment and theoretical correlation study, *ACS Sensors* 1 (4) (2016) 406–412.
- [35] B. Ruhland, T. Becker, G. Müller, Gas-kinetic interactions of nitrous oxides with SnO<sub>2</sub> surfaces, *Sensors Actuat. B: Chem.* 50 (1) (1998) 85–94.
- [36] M. Chen, Z. Wang, D. Han, F. Gu, G. Guo, High-sensitivity NO<sub>2</sub> gas sensors based on flower-like and tube-like ZnO nanomaterials, *Sensors Actuat. B: Chem.* 157 (2) (2011) 565–574.
- [37] M.-W. Ahn, K.-S. Park, J.-H. Heo, J.-G. Park, D.-W. Kim, K.J. Choi, J.-H. Lee, S.-H. Hong, Gas sensing properties of defect-controlled ZnO-nanowire gas sensor, *Appl. Phys. Lett.* 93 (26) (2008) 263103.
- [38] F. Fan, Y. Feng, S. Bai, J. Feng, A. Chen, D. Li, Synthesis and gas sensing properties to NO<sub>2</sub> of ZnO nanoparticles, *Sensors Actuat. B: Chem.* 185 (2013) 377–382.
- [39] M. Chen, Z. Wang, D. Han, F. Gu, G. Guo, Porous ZnO polygonal nanoflakes: synthesis, use in high-sensitivity NO<sub>2</sub> gas sensor, and proposed mechanism of gas sensing, *J. Phys. Chem. C* 115 (26) (2011) 12763–12773.